ISSN 1392-1320 MATERIALS SCIENCE (MEDŽIAGOTYRA). Vol. 31, No. 2. 2025

Experimental Study on the Dynamic Compressive Response of Sand with Respect to Relative Density and Water Content

Shuping SUN [1] *, Shu SUN [2], Qingxian YU [3], Yongchun LI [3], Xinwen QIAN [1]

[1] *School of Architecture and Environmental Engineering, Silicon Lake College, Suzhou, 215332, Jiangsu, China*
[2] *School of Architecture and Engineering, Taizhou Polytechnic College, Taizhou, 225300, Jiangsu, China*
[3] *Beijing Jianghe Curtain Wall System Engineering Co., Ltd, Shunyi, 101300, Beijing, China*

http://doi.org/10.5755/j02.ms.38365

Received 5 August 2024; accepted 27 September 2024

This paper presents the findings of dynamic compression tests conducted on sand specimens utilizing a ∅ 100 mm Split Hopkinson Pressure Bar (SHPB) apparatus. The study aims to investigate the dynamic response characteristics of sand with varying relative densities and water contents subjected to different strain rates. The test results indicate a significant effect of strain rate on the dynamic response of sand. Initially, the equivalent stiffness of sand increases linearly with the strain rate; however, once the strain rate exceeds 381 s^{-1}, this stiffness exhibits a marked enhancement. For dry sand specimens, the peak stress gradually increases with strain rate. Conversely, for specimens with varying water contents, peak stress initially increases and subsequently decreases as the strain rate rises. The strain corresponding to peak stress is influenced by the combined effects of water content and relative density, exhibiting an initial increase followed by a decrease as the strain rate rises. When relative density remains constant at 0.9, the energy absorption density increases linearly with water content, peaking at 6.0 %. Furthermore, a positive correlation exists between the compression wave velocity of the specimens and both water content and relative density. Specifically, as water content increases from 0 – 10 %, the average compression wave velocity rises by 107.0 %. Similarly, as relative density increases from 0.1 – 0.9, the wave velocity of the sand specimens increases by 96.4 %. These findings suggest that optimizing water content can enhance the energy absorption capacity of sand within the energy absorption layers of protective structures.

Keywords: sand, high strain rate, relative density, water content, split Hopkinson pressure bar.

1. INTRODUCTION

Sand comprises a skeleton of discrete solid particles and numerous small, densely grouped pores interspersed within the skeleton, exhibiting typical characteristics of a two-phase solid-fluid system, thereby rendering it a complex non-equilibrium energy-dissipative medium [1]. Due to its porous, loose, and highly compressible nature, stress waves in sandy media exhibit significant dispersion and attenuation under explosive, impact, and vibrational loads [2], which makes it widely utilized as an energy absorption distribution layer in protective structures, including military defense engineering [3, 4] and buffer layers for rockfall impact protection sheds (retaining walls) [5 – 8]. Additionally, the response of soil to dynamic stress is pertinent in fields such as dynamic compaction of foundations [9] and vibroflotation pile foundation engineering [10]. Unlike solid materials, the strength of sand markedly increases under dynamic loads, exhibiting clear strain rate dependence attributable to its solid-fluid characteristics [11]. During dynamic compression, larger pores promote particle breakage. As particles fracture, the pores within the soil skeleton diminish, altering the contact configuration between broken particles, which leads to a significant increase in stiffness [12]. This transition from an initially highly compressible "fluid-like state" to a less compressible "solid-like state" demonstrates a dense, rock-like characteristic [13]. Considering the various physical and mechanical states of sand under different site and environmental conditions, such as water content and compaction state, it is essential to investigate the mechanical response of sand to dynamic loads. This research aims to derive mechanical parameters of sand at high strain rates, thereby providing a scientific basis for seismic design and blast-resistant engineering.

The Split Hopkinson Pressure Bar (SHPB) is an effective experimental method for investigating the dynamic compressive properties of engineering materials under medium to high strain rates (10^{-2} to 10^{-4} s^{-1}) [14 – 16]. It is a crucial component of impact dynamics experimental technology. As early as 1967, Fletcher et al. [17] conducted an initial study on the dynamic characteristics of soil using SHPB. Since soil is a granular material, a sleeve and pad are required to secure the soil sample during the experiment. The soil sample is placed between the pads, akin to a "sandwich," while high-sensitivity strain gauges attached to the incident and transmission bars record the stress and strain time-history curves of the sample [18]. Lin et al. [19] analyzed one-dimensional quasi-static and SHPB impact tests on Ottawa sand, finding that the strain rate effect of dry sand increases with higher strain levels. Luo et al. [20] conducted SHPB impact tests on glass beads to examine the effects of initial mass density, particle size, and water content on dynamic volumetric strain and deviatoric strain. Lv et al. [21 – 23] conducted one-dimensional quasi-static and SHPB impact tests on calcareous sand and quartz sand,

* Corresponding author: S. Sun
E-mail: *12011002@usl.edu.cn*

revealing the strain rate effect and the particle breakage characteristics of calcareous sand. Song et al. [24] utilized sleeves of varying materials to modify the lateral confinement conditions of sand and conducted SHPB tests on dry sand with different relative densities, concluding that the dynamic compressive properties of sand are primarily influenced by relative density and lateral confinement conditions, and that the strength of the sleeve material is proportional to the axial bearing capacity of the sample. Zhao et al. [25] also demonstrated that density is a primary factor influencing the dynamic compressive properties of sand. Wang et al. [26] conducted impact tests on Stockton Beach sand and glass beads under passive confinement conditions, with the results indicating that the strain rate effect of dry specimens is not significant.

Previous research has established a solid foundation for conducting SHPB tests on soil; however, due to the complexity of the dynamic characteristics of sand, the conclusions drawn by various scholars based on experimental studies are not entirely consistent. Furthermore, unlike solid materials, granular materials cannot be subjected to loading through direct clamping with the incident and transmission bars. Accurate control of the initial density is also a crucial factor influencing the dynamic response of the sample [27]. This paper enhances the Split Hopkinson Pressure Bar by designing a device that can accurately control the length and relative density of granular material specimens. In this setup, the granular sand particles are positioned within a steel sleeve exhibiting ideal rigidity. Given that the sleeve does not induce lateral strain on the sample, it can be approximated that the experiment adheres to the one-dimensional strain assumption [28]. Therefore, this study investigates the influence of relative density and water content on the dynamic compressive properties of sand under moderate to high strain rates.

2. EXPERIMENTAL DESIGN

2.1. Test equipment

The SHPB device is an equal cross-section bar system with a diameter of 1000 mm, and an enhanced long sleeve device has been designed for testing granular particles (Fig. 1). The SHPB primarily comprises a loading system, a pressure bar system, and a data acquisition module. The loading system propels a bullet to impact the incident bar by compressing nitrogen gas, and the bullet's speed can be regulated by adjusting the air pressure. The pressure bar system comprises an incident bar and a transmission bar, with lengths of 4850 mm and 3000 mm, respectively. The material utilized is 35CrMnSi high-strength steel, characterized by an elastic modulus of 206 GPa, an elastic wave propagation speed of 5100 m/s, a density of 7.84 $g{\cdot}cm^{-3}$, and a yield strength of 1280 MPa. Furthermore, considering the low and variable wave impedance of the granular materials tested in this study, high-sensitivity semiconductor strain gauges with a resistance value of 120 Ω and a gain factor of 1000 are employed in the experiment. The distance between the semiconductor strain gauge and the front end of the specimen measures 2500 mm, while the distance between the strain gauge on the transmission bar and the rear end of the specimen measures 1500 mm.

A loading sleeve optimized for granular materials has been designed, primarily consisting of an inner sleeve, an outer sleeve, and a support platen. The outer sleeve is composed of 35CrMnSi high-strength steel, featuring an inner diameter of 101 mm, an outer diameter of 111 mm, and a wall thickness of 10 mm. This sleeve provides lateral constraint to the granular material while permitting the incident bar to slide and rotate within it. The inner sleeve, constructed from the same material, has an inner diameter of 80 mm and an outer diameter of 85 mm, serving to facilitate precise control of the sample length. The platens comprise a front-end platen, a rear-end platen, and a support platen. The platens are fabricated from the same material as the SHPB and have a diameter of 10 mm. The primary function of the front and rear platens is to eliminate discontinuities between the specimen and the bar ends while securing the granular material during loading and handling. The support platen is positioned at the base of the rear platen to prevent deformation during pre-compression, which may adversely affect experimental accuracy. Additionally, to achieve improved stress balance and enhanced waveform quality, a shaper may be attached to the front end of the incident bar. The primary function of the shaper is to increase the rise time, facilitating multiple reflections of the stress wave to achieve stress balance more rapidly [29, 30]. In this study, annealed brass with a diameter of 20 mm is employed as the shaper.

2.2. Test materials and specimen preparation

The sand utilized in the experiment is standard river sand sourced from Jiangsu Province, with SiO_2 as the primary component. An indoor sieving test was conducted on the sand sample.

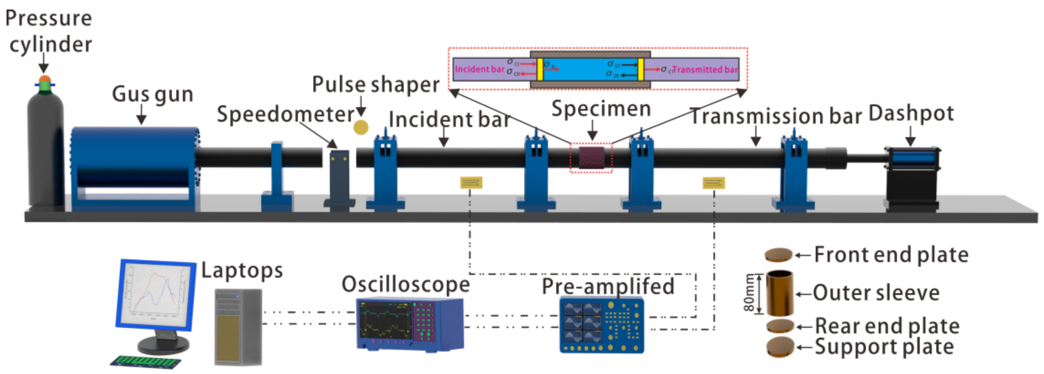

Fig. 1. Improved SHPB

Based on the mass proportion of each particle group after sieving, a gradation curve was plotted, as illustrated in Fig. 2. To minimize errors and ensure sample uniformity, only particles with diameters ranging from 1.0 to 2.5 mm were selected for the impact test. The final specific gravity of the sand utilized in the test is 2.6, with a maximum dry density of 1.76 g•cm^{-3} and a minimum dry density of 1.6 g•cm^{-3}.

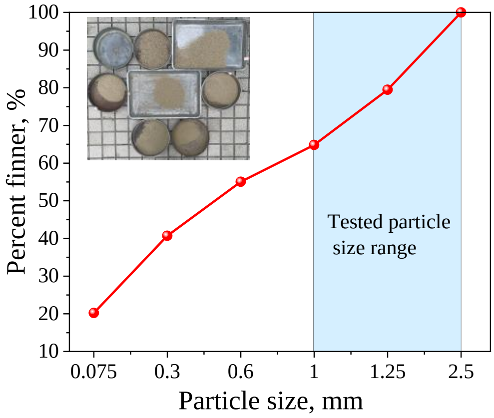

Fig. 2. Particle size distribution

Before preparing the sample, the inner wall of the sleeve is uniformly coated with graphite. The graphite significantly reduces friction between the sample and the inner wall of the sleeve, thereby ensuring uniform radial pressure transfer between the sleeve and the sample. Subsequently, based on the specified sample density, a precise amount of sand is weighed and placed into the sleeve. To prevent alterations in the water content of the sample, the confinement cylinder is promptly installed on the bar following the completion of sample preparation, thereby ensuring that the end face of the pressure bar is in close contact with the sample.

2.3. Test procedure

In SHPB experiments, the longitudinal and radial inertia effects of the specimen can influence the stress-strain results to a certain degree; therefore, the recommended length-to-diameter ratio of the specimen is between 0.4 and 0.6 [31, 32]. According to Song et al. [33], who analyzed factors affecting stress equilibrium in soft materials, thinner specimens are more likely to achieve stress equilibrium; however, excessively thin specimens may introduce experimental errors due to increased friction between the pressure bar and the specimen's end face. In light of these considerations, a length-to-diameter ratio of 0.5, corresponding to a specimen length of 50 mm, was selected for this experiment. Once the specimen's length and diameter are established, its volume can subsequently be calculated. Under fixed volume conditions, varying specimen masses are utilized to produce sand specimens with differing densities. Various water contents are achieved by incorporating different masses of water into the specimens. The specific experimental steps are outlined in Fig. 3:

1. Place the support platen on a horizontal surface and stack the rear end platen on top of the support platen. Secure the sleeve with the rear end plate using screws.
2. Pour the sand sample evenly into the sleeve, lightly compact it, and slowly slide the front end platen down to the top of the specimen to ensure air is expelled from the sleeve.

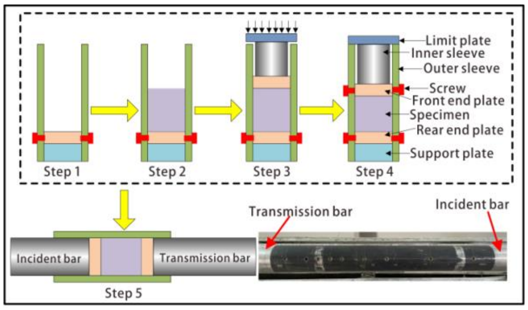

Fig. 3. Test steps

3. Place the inner sleeve on the front platen and then uniformly pre-compress the specimen until the inner sleeve is flush with the top of the outer sleeve.
4. Remove the inner sleeve and secure the front end plate with screws to prevent changes in the length and density of the specimen during handling.
5. Place the specimen between the incident and transmission bars, ensuring the sleeve is level and full contact is maintained between the end face of the incident bar and the end face of the front end platen.

3 RESULTS AND ANALYSIS

3.1. Experimental effects analysis

Fig. 4 presents the measured waveforms of the incident, reflected, and transmitted waves.

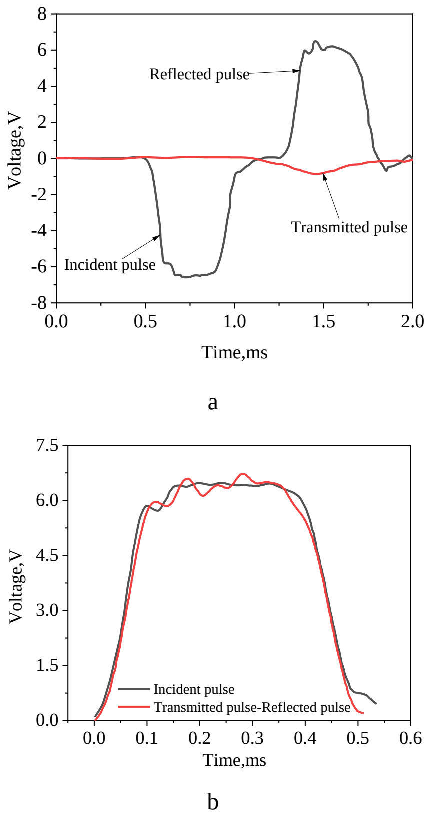

Fig. 4. Effectiveness analysis of the test: a – raw waveform; b – stress equilibrium

The waveforms exhibit a smooth trend with no significant oscillations, indicating minimal mutual superposition effects in the stress waves within the specimen. The typical waveforms obtained in this experiment demonstrate that the incident wave lasts approximately 632 μs, the reflected wave approximately 597 μs, and the transmitted wave approximately 693 μs. The durations of these three waves are nearly equal, and the voltage signals of the incident and reflected waves align closely with the voltage signal of the transmitted wave (Fig. 4 a). The results presented in Fig. 4 b indicate that the stress equilibrium assumption is satisfied at any given moment. Consequently, this experiment confirms the establishment of uniform stress distribution and momentum conservation, thereby validating the reliability of the experimental results.

3.2. Stress-strain curve

Utilizing the incident, reflected, and transmitted strain signals from the incident and transmission bars, and based on the two fundamental assumptions of the SHPB experiment, the collected raw waveforms are processed using the three-wave method [34] to derive the expressions for the specimen's stress σ(t), strain ε(t), and strain rate $\dot{\varepsilon}$, respectively, as follows:

$$\begin{cases} \sigma(t) = \dfrac{2AE_0}{2A_s}\left[\varepsilon_i(t) + \varepsilon_r(t) + \varepsilon_t(t)\right] \\ \varepsilon(t) = \displaystyle\int_0^t \dfrac{C_0}{l_s}\left[\varepsilon_i(t) - \varepsilon_r(t) - \varepsilon_t(t)\right]dt \\ \dot{\varepsilon}(t) = \dfrac{C_0}{l_s}\left[\varepsilon_i(t) - \varepsilon_r(t) - \varepsilon_t(t)\right] \end{cases}, \qquad (1)$$

where ε_i, ε_r, and ε_t denote the strain signals of the incident, reflected, and transmitted waves, respectively; $\dot{\varepsilon}$ denotes the strain rate; E_0 signifies the elastic modulus of the bar; A and A_s denote the cross-sectional areas of the bar and the specimen; C_0 indicates the wave velocity in the pressure bar, and l_s represents the length of the specimen.

Fig. 5 shows the comparative results of dynamic compression stress-strain curves of sand specimens under different strain rate conditions. Sand exhibits a significant strain rate effect under dynamic compression conditions. The dynamic response characteristics vary notably across different strain rates. As the strain rate increases, there is a gradual rise in peak stress, indicating a strengthening effect due to the strain rate.

To further quantify the dynamic strength of the material under strain rate conditions, this study introduces the concept of equivalent stiffness.

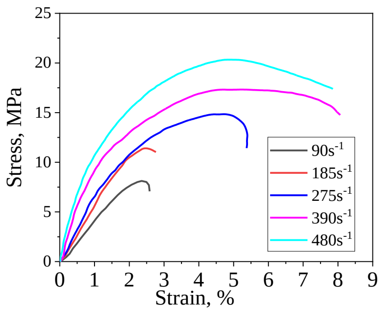

a

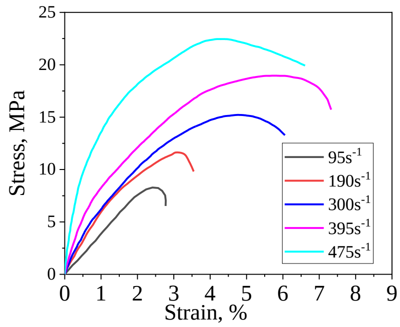

b

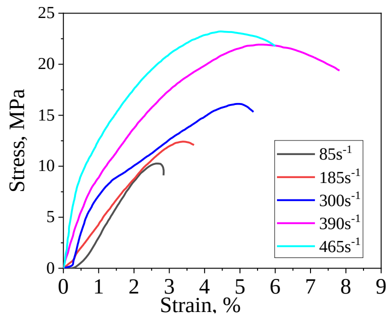

c

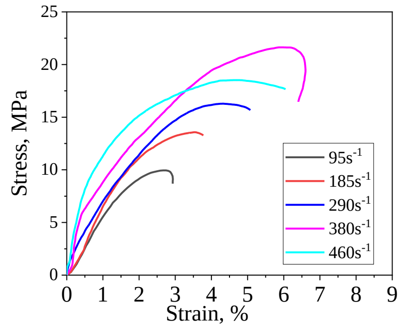

d

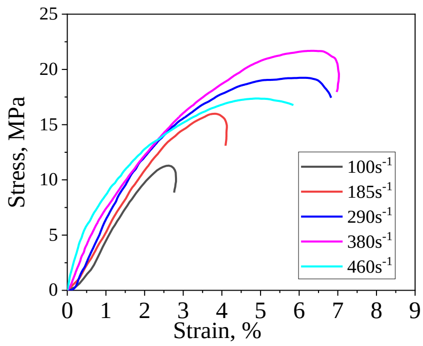

e

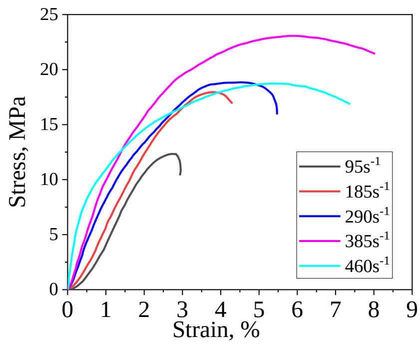

f

continued on next page

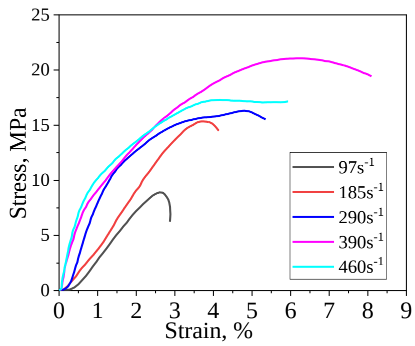

g

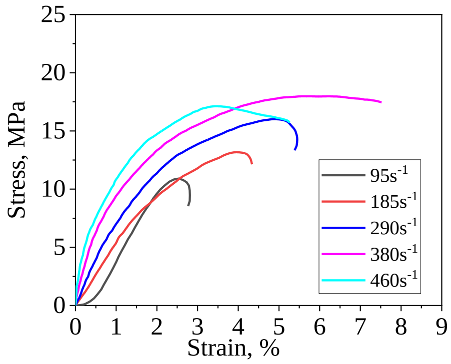

h

Fig. 5. Stress-strain response of sand at different strain rates: a – w = 0.0 %, D_r = 0.1; b – w = 0.0 %, D_r = 0.6; c – w = 0.0 %, D_r = 0.9; d – w = 2.0 %, D_r = 0.9; e – w = 4.0 %, D_r = 0.9; f – w = 6.0 %, D_r = 0.9; g – w = 8.0 %, D_r = 0.9; h– w=10.0%, D_r=0.9

The equivalent stiffness characterizes the sand sample's resistance to deformation and essentially represents the secant modulus at 50 % of the peak dynamic stress. The equivalent stiffness is defined as follows [35]:

$$E_{50} = \frac{\sigma_{50}}{\varepsilon_{50}}, \tag{2}$$

where E_{50} is the equivalent stiffness of the sand; σ_{50} is the stress at 50 % of the peak dynamic stress point of the sand, and ε_{50} is the strain corresponding to σ_{50}.

Fig. 6 illustrates the variation of equivalent stiffness of specimens with strain rate under different impact conditions.

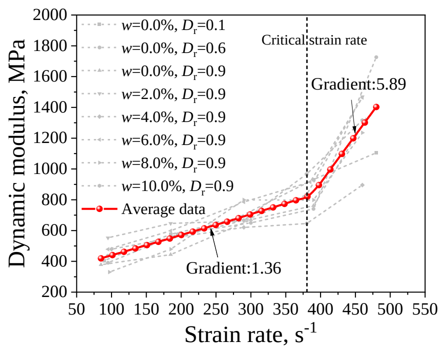

Fig. 6. Equivalent stiffness variation characteristics

The results indicate that, under different water contents and relative densities, the variation of equivalent stiffness with increasing strain rate can be divided into two stages. In the first stage, at strain rates below 381 s^{-1}, equivalent stiffness shows a linear increase with strain rate, with a gradient of 1.36. In the second stage, at strain rates above 381 s^{-1}, equivalent stiffness also exhibits a linear increase with strain rate, but with a gradient of 5.89. It is evident that there exists a critical value for the impact of strain rate on the equivalent stiffness of the material. When the strain rate is below this critical value, particle fragmentation is minimal, and the compression of the specimen is primarily caused by the sliding deformation of the particles [36]. However, when the strain rate surpasses the critical value, the particles experience extensive fragmentation, leading to a significant decrease in porosity and an increase in the particle contact area. Moreover, at higher strain rates, the discharge of water from the specimens becomes more challenging compared to lower strain rates. Consequently, the presence of pore water hampers the compressive deformation of the specimens [37]. In the second stage, all specimens exhibit a decrease in peak stress compared to the initial stage (Fig. 5). However, the rate of peak stress decrease is smaller than the rate of strain decrease, thereby indicating a more pronounced increase in the rate of equivalent stiffness compared to the first stage.

Concerning the strain rate effect on sand, Lv et al. [21] and Song et al. [24] indicated that the compression response of sand is generally insensitive to strain rate. Conversely, Lin et al. [19] observed in a compression study involving two types of Ottawa Sands that the strain rate effect becomes more pronounced following particle fragmentation and rearrangement, which is more closely aligned with the findings of this study.

3.3. Effect of relative density

Fig. 7 depicts the relationship between peak stress and strain rate under varying conditions. The results indicate that, for dry sand specimens exhibiting varying relative densities and approximately constant strain rates, dynamic peak stress increases as specimen density increases. This phenomenon arises from the denser packing of sand particles, larger contact areas between them, and enhanced frictional forces, which reduce particle sliding and improve specimen compression resistance. In contrast, sand specimens with a controlled relative density of 0.9, differing in water content, demonstrate a peak stress trend with a strain rate that initially increases and subsequently decreases. For unsaturated specimens, the peak stress first increases and then decreases with increasing strain rate. When the strain rate is less than 381 s^{-1}, the peak stress consistently increases with increasing strain rate; however, when the strain rate exceeds 381 s^{-1}, the peak stresses of all specimens decrease. As previously mentioned, pore water is more challenging to discharge under high strain rate conditions compared to low strain rates[38]. When the strain rate exceeds a critical threshold, pore water absorbs a portion of the external load, resulting in a decrease in peak stress for the specimens. Although the change in effective stress during impact could not be quantified in this test, according to the principle of effective stress[37], the external load is predominantly supported by the sand skeleton under well-drained conditions; however, pore water pressure significantly increases and effective stress decreases when rapidly loaded or when drainage conditions are inadequate. Therefore, under elevated strain rate loading conditions, the variation in peak stress of the specimen can be qualitatively explained by the principle of effective stress.

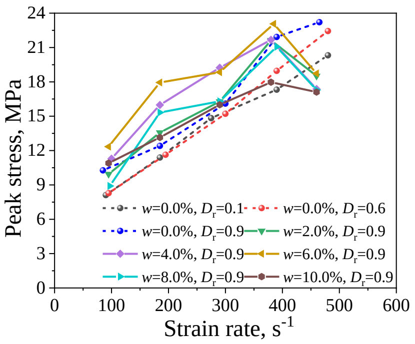

Fig. 7. Relationship between peak stress and strain rate

Fig. 8 illustrates the relationship between peak strain and strain rate under different conditions. The results indicate that the influence of strain rate on peak strain remains consistent for both wet and dry sand, irrespective of differing relative densities.

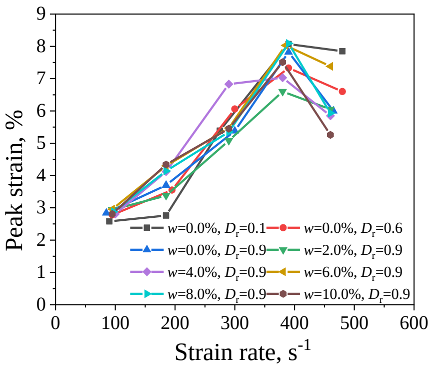

Fig. 8. Relationship between peak strain and strain rate

Throughout the tested range of strain rates, the peak strain of sand specimens exhibiting different relative densities initially increases and subsequently decreases. Specifically, when the applied strain rate is below the critical threshold, the peak strain increases approximately linearly with the rising strain rate. Conversely, when the applied strain rate exceeds the critical threshold, the peak strain decreases as the strain rate increases. This trend arises because, at lower strain rates below the critical threshold, sand particles experience a minimal fracture, and deformation primarily involves particle sliding and rolling. However, as the strain rate surpasses a critical threshold, resulting in particle fragmentation, numerous particles fracture within the specimen. The resulting finer particles occupy certain voids in the specimen, thereby reducing its overall deformation capacity. Furthermore, pore water impedes the compressive deformation of the specimen more significantly at elevated strain rates compared to low strain rate conditions.

Established studies have shown that, under conditions of smaller strain rates, the degree of particle fragmentation is low. The compressive deformation of the specimen is primarily dominated by particle slippage and pore reduction [20]. As the strain rate increases, particle fragmentation occurs, particularly because the stiffness of larger particles is lower than that of fine particles, and larger particles tend to have more initial defects [39]. Consequently, the fragmentation effect becomes more pronounced. The debris generated from the crushing of larger particles fills the pores, reducing the pore ratio of the specimen, which, in turn, leads to a significant decrease in the specimen's deformation capacity [40].

3.4. Effect of water content

Fig. 9 and Fig. 10 illustrate the variations of peak stress and strain with water content under different strain rate conditions.

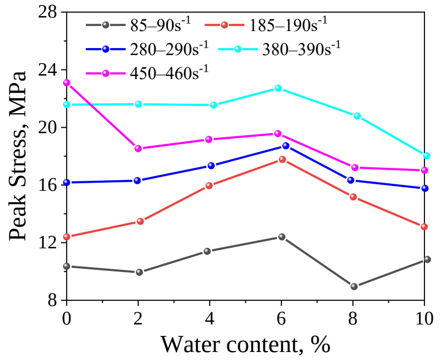

Fig. 9. Effect of water content on peak stress

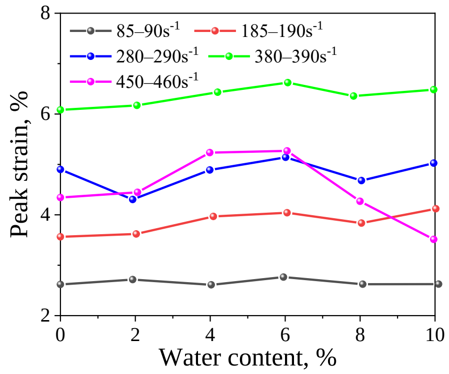

Fig. 10. Effect of water content on peak strain

Both peak stress and the corresponding peak strain show a non-monotonic relationship with increasing water content, initially rising and then declining. This pattern suggests the presence of a critical water content threshold: below this threshold, both peak stress and peak strain increase with water content; however, above it, both decrease. In this study, conducted under specific experimental conditions, the critical water content threshold for sand specimens with a relative density of 0.9 is determined to be 6.0 %.

3.5. Energy absorption effect

Sand, as a typical porous material, exhibits critical energy absorption characteristics that significantly impact its mechanical properties. The area beneath the stress-strain curve represents the energy absorbed per unit volume of the material during elastic deformation [41,42], often referred to as toughness. The specific expression is given by:

$$\eta = \int_0^{\varepsilon} \sigma d\varepsilon \cdot \tag{3}$$

Fig. 11 shows the variation of energy density with water content. The results show that at a relative density of 0.9, the energy density of the sample initially increases and then decreases with rising water content. For dry sand, tested at strain rates from 85–465 s^{-1}, the average energy density measures 0.4977 $MJ \cdot m^{-3}$. Increasing water content to 6.0 % under strain rates of 95–460 s^{-1} significantly boosts the average energy density to 0.5772 $MJ \cdot m^{-3}$, marking a notable increase of 15.97 % in absorbed energy density. However, further increases in water content lead to a gradual decrease in absorbed energy density. At 10.0 % water content and strain rates of 95–460 s^{-1}, the average energy density drops to 0.4416 $MJ \cdot m^{-3}$, which is 23.49 % lower compared to the maximum value. This highlights the importance of maintaining the ideal water content to improve the energy absorption capacity of sand particles in the energy absorption layers of protective structures.

Xiong et al. [43] conducted a comparative analysis of the effects of water content in quartz sand and silica sand on energy absorption efficiency, showing that increasing the water content of the dispersion layer can improve efficiency. Additionally, Tong et al. [44] studied the mechanical response of loess to impact loading and found that near optimum water content, the pore water plays the role of bearing part of the impact load, enhancing the material's ability to dissipate impact energy. These findings are consistent with the results presented in this paper.

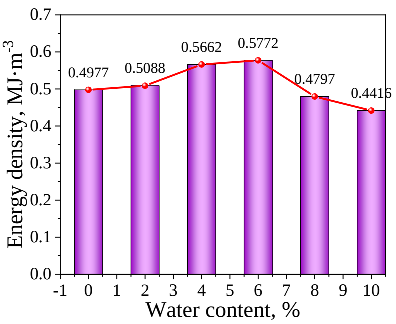

Fig. 11. Effect of water content on energy density

Fig. 12 illustrates the relationship between energy density and sample relative density.

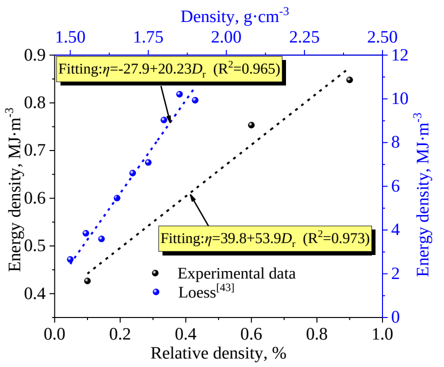

Fig. 12. Effect of relative density on energy density

The results show that, with constant water content, energy density increases linearly with the material's relative density. Energy densities at relative densities of 0.1, 0.6, and 0.9 are 0.4265 $MJ \cdot m^{-3}$, 0.7533 $MJ \cdot m^{-3}$, and 0.8484 $MJ \cdot m^{-3}$, respectively. Higher relative density leads to denser packing of soil particles and increased frictional forces between them. This increased frictional resistance between solid particles plays a crucial role in resisting deformation and particle slippage within the material's closed volume. Consequently, higher sample density absorbs more energy, enhancing the material's energy absorption capacity. The relationship between relative density and energy density is further fitted using a linear function, which can be expressed as:

$$\eta = 53.9\, D_r + 39.8, \tag{4}$$

where η is the energy density; D_r is the relative density.

In addition, Xiong et al. [43] conducted a study on loess specimens with a strain rate of 445 s^{-1} and a water content of 3.77 %. The findings revealed that increasing the initial density from 1.5–1.90 $g \cdot cm^{-3}$ resulted in an increase in the corresponding energy density from 2.7–9.87 $MJ \cdot m^{-3}$. This increase in energy density follows a linear relationship with the initial density, which supports the conclusion of this paper.

3.6. Stress wave velocity

Stress wave is the propagation form of disturbance caused by stress in a medium's particles. The stress wave velocity is of significant importance in studying the propagation laws of waves and the dynamic physical parameters of materials. Based on the stress wave time history curve in the SHPB, combined with the specimen length, the compression wave velocity C of the stress wave in granular media can be calculated. The calculation expression is:

$$C = \frac{l_s}{\Delta t - t_1 - t_2}, \tag{5}$$

where Δt is the time difference between the strain gauge signals on the incident bar and the transmission bar, t_1 is the time for the stress wave to propagate from the strain gauge in the incident bar to the front end of the specimen, and t_2 is the time for the stress wave to propagate from the rear end of the specimen to the strain gauge in the transmission bar.

Fig. 13 illustrates the compression wave velocities of the specimens under different impact conditions.

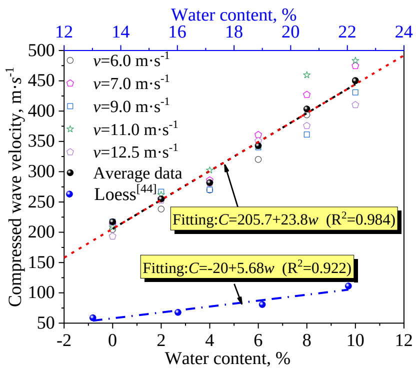

Fig. 13. Effect of water content on wave velocity

It can be observed that, for specimens with the same water content, the compression wave velocities remain consistent across various loading rates. This implies that the impact velocity has a minimal influence on the compression wave velocity of sand. In addition, further analysis is conducted to calculate the average compression wave velocity, which revealed that water content plays a significant role in determining the velocity. Higher water content correlates positively with increased compression wave velocities in the specimen, which can be expressed as:

$$C=23.8\,w+205.7, \tag{6}$$

where w is the water content.

The fitting results indicate the correlation coefficient of 0.984 for the fitted equation, despite the presence of a discrete pattern in the data. This suggests that the compression wave velocity is only minimally affected by the loading speed. In addition, According to Tong et al. [44], the velocity of compression waves in remodeled loess at impact velocities of 4 – 10 m·s^{-1} increases in a nearly linear fashion with increasing water content. Moreover, the average velocity of compression waves in the specimens increases by 103.4 % as the water content in the loess increases from 13 – 22 %. In comparison to the unsaturated sand specimens discussed in the present study, the stress wave propagation speed in the sand is greater than that in loses due to differences in mineral composition, particle shape, and porosity. However, both loess and sand specimens demonstrate an approximately linear relationship between compression wave velocity and water content.

Fig. 14 illustrates the influence of relative density on the compression wave velocity.

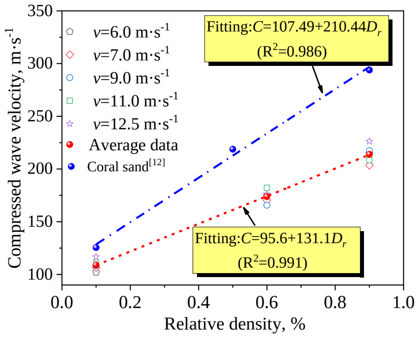

Fig. 14. Effect of relative density on wave velocity

The results show that the compression wave velocity of the specimen is approximately linearly correlated with the material's relative density, at a relative density of 0.1, the average wave velocity of the specimen is 108.9 m·s^{-1}, whereas it increases to 213.9 m·s^{-1} when the relative density increases to 0.9, representing an increase of 96.4 %. The fitting equation can be expressed as:

$$C=131.1\,D_r+95.6. \tag{7}$$

In addition, Yu et al. [12] reported the change rule of compression wave velocity in three cases of relative density of 0.1, 0.5 and 0.9 respectively showed that the wave velocity and the relative density of the specimen are in good linear relationship, which is basically consistent with the results of this paper.

4 CONCLUSIONS

1. The stress-strain relationship of sand exhibits characteristic nonlinear behavior, indicating that the material experiences a pronounced strain rate effect. The equivalent stiffness of sand increases with increasing strain rate. When the strain rate exceeds 381 s^{-1}, the equivalent stiffness of the specimen exhibits a strengthening effect.
2. At approximately the same strain rate, higher specimen density results in an increase in dynamic peak stress. However, as water content varies, peak stress initially increases and subsequently decreases with increasing strain rate. Similarly, for both dry and wet sand, peak strain tends to increase and subsequently decrease as the strain rate increases.
3. When the water content of the specimen is below the critical threshold, both peak stress and strain increase as the water content rises. Conversely, when the water content exceeds the critical threshold, both peak stress and strain decrease with further increases in water content.
4. The energy density of the specimens initially increases with water content, peaking at a critical water content of 6.0 % before subsequently decreasing. This peak represents a 15.97 % increase compared to dry sand and a 30.71 % increase compared to the energy density at 10.0 % water content. Consequently, optimal water content enhances the energy absorption capacity of sand within the energy absorption layer of the protective structure. Furthermore, at a constant water content, energy density exhibits a linear positive correlation with the material's relative density.
5. The compression wave velocity of the specimen exhibits a positive correlation with water content. Increasing water content from 0 – 10.0 % results in a 107.0 % increase in wave velocity. Similarly, higher relative densities correspond to higher wave velocities, increasing by 96.4 % as relative density rises from 0.1 – 0.9.

REFERENCES

1. **Jaegeer, H.M., Nagel, S.R., Behringer, R.P.** Granular Solids, Liquids, and Gases *Reviews of Modern Physics* 68 (4) 1996: pp. 1259 – 1273. https://doi.org/10.1103/RevModPhys.68.1259
2. **Li, J.C., Ma, G.W.** Experimental Study of Stress Wave Propagation Across a Filled Rock Joint *International Journal of Rock Mechanics and Mining Sciences* 46 (3) 2009: pp. 471 – 478. https://doi.org/10.1016/j.ijrmms.2008.11.006
3. **Wang, Z., Lu, Y.** Numerical Analysis on Dynamic Deformation Mechanism of Soils Under Blast Loading *Soil Dynamics and Earthquake Engineering* 23 (8) 2003: pp. 700 – 714. https://doi.org/10.1016/S0267-7261(03)00076-9
4. **Bragov, A.M., Lomunov, A.K., Sergeichev, I.V., Tsembelis, K., Proud, W.G.** Determination of Physicomechanical Properties of Soft Soils From Medium to High Strain Rates *International Journal of Impact Engineering* 35 (9) 2008: pp. 967 – 976. https://doi.org/10.1016/j.ijimpeng.2007.07.004
5. **Zhao, D.B., Yi, W.J., Kunnath, S.K.** Numerical Simulation and Shear Resistance of Reinforced Concrete Beams Under Impact *Engineering Structures* 166 2018: pp. 387 – 401. https://doi.org/10.1016/j.engstruct.2018.03.072
6. **Claudio, D.P., Vecchiotti, M.** Design Charts for Evaluating Impact Forces on Dissipative Granular Soil Cushions *Journal of Geotechnical and Geoenvironmental Engineering* 136 (11) 2010: pp. 1529 – 1541.

https://doi.org/10.1061/(ASCE)GT.1943-5606.0000363

7. **Pichler, B., Hellmich, C., Mang, H.A.** Impact of Rocks onto Gravel Design and Evaluation of Experiments *International Journal of Impact Engineering* 31 (5) 2005: pp. 559 – 578. https://doi.org/10.1016/j.ijimpeng.2004.01.007
8. **Bhatti, A.Q., Kishi, N.** Impact Response of RC Rock-shed Girder with Sand Cushion Under Falling Load *Nuclear Engineering and Design* 240 (10) 2010: pp. 2626 – 2632. https://doi.org/10.1016/j.nucengdes.2010.07.029
9. **Gu, Q., Lee, F.H.** Ground Response to Dynamic Compaction of Dry Sand *Geotechnique* 52 (7) 2002: pp. 481 – 493. https://doi.org/10.1680/geot.2002.52.7.481
10. **Jafarian, Y., Mehrzad, B., Lee, C.J., Haddad, A.H.** Centrifuge Modeling of Seismic Foundation-soil-foundation Interaction on Liquefiable Sand *Soil Dynamics and Earthquake Engineering* 97 2017: pp. 184 – 204. https://doi.org/10.1016/j.soildyn.2017.03.019
11. **Kuang, D., Long, Z., Guo, R., Yu, P.** Experimental and Numerical Investigation on Size Effect on Crushing Behaviors of Single Calcareous Sand Particles *Marine Georesources and Geotechnology* 39 (5) 2020: pp. 543 – 553. https://doi.org/10.1080/1064119X.2020.1725194
12. **Yu, X., Chen, L.,Fang, Q., Zhang, J.H., Guo, D., Hou, X.F.** Determination of Attenuation Effects of Coral Sand on the Propagation of Impact-induced Stress Wave *International Journal of Impact Engineering* 125 2019: pp. 63 – 82. https://doi.org/10.1016/j.ijimpeng.2018.11.004
13. **Omidvar, M., Iskander, M., Bless, S.** Stress-strain Behavior of Sand at High Strain Rates *International Journal of Impact Engineering* 49 2012: pp. 192 – 213. https://doi.org/10.1016/j.ijimpeng.2012.03.004
14. **Kolsky, H.** An Investigation of the Mechanical Properties of Materials at Very High Rates of Loading *Proceedings of the Physical Society: Section B* 62 (11) 1949: pp. 676 – 700. https://doi.org/10.1088/0370-1301/62/11/302.
15. **Huang, J, Xu, S, Hu, S.** Effects of Grain Size and Gradation on the Dynamic Responses of Quartz Sands *International Journal of Impact Engineering* 59 (9) 2013: pp. 1 – 10. https://doi.org/10.1016/j.ijimpeng.2013.03.007
16. **Chen, H., Zhang, C., Wei, J.Q.,Wang, Y.M.** A Modified Method for Estimating the Stress State of Granular Materials in the Passive Confined Pressure SHPB Tests *International Journal of Impact Engineering* 160 2022: pp. 104063. https://doi.org/10.1016/j.ijimpeng.2021.104063
17. **Fletcher, E., Poorooshasb, H.** Response of a Clay Sample to Low Magnitude Loadsapplied at High Rate *Proceedings of the International Symposium on Wavepropagation and Dynamic Properties of Earth Materials* 1967: pp. 86 – 781.
18. **Einav, I.** Breakage Mechanics−Part I: Theory *Journal of the Mechanics and Physics of Solids* 55 (6) 2007: pp. 1274 – 1297. https://doi.org/10.1016/j.jmps.2006.11.003
19. **Lin, Y., Yao Jafari, W., Wang, M., Xia, N.K.** Quantification of the Dynamic Compressive Response of Two Ottawa Sands *Experimental Mechanics* 57 (9) 2017: pp. 1371 – 1382. https://doi.org/10.1007/s11340-017-0304-0
20. **Luo, H., Du, Y., Hu, Z., Lu, H.** High-strain Rate Compressive Behavior of Glass Beads Under Confinement *Experimental Mechanics* 55 (5) 2015: pp. 935 – 950. https://doi.org/10.1007/s11340-015-9995-2
21. **Lv, Y.R., Liu, J.G., Xiong, Z.M.** One-dimensional Dynamic Compressive Behavior of Dry Calcareous Sand at High Strain Rates *Journal of Rock Mechanics and Geotechnical Engineering* 11 (1) 2019: pp. 3209 – 3228. https://doi.org/10.1016/j.jrmge.2018.04.013
22. **Lv, Y.R., Liu, J.G., Zuo, D.J.** Moisture Effects on the Undrained Dynamic Behavior of Calcareous Sand at High Strain Rates *Geotechnical Testing Journal* 42 (3) 2018: pp. 20170412. https://doi.org/10.1520/GTJ20170412
23. **Lv, Y.R., Li, X., Fan, C.F., Su, Y.** Effects of Internal Pores on the Mechanical Properties of Marine Calcareous Sand Particles *Acta Geotechnica* 16 (10) 2021: pp. 3209 – 3228. https://doi.org/10.1007/s11440-021-01223-8
24. **Song, B., Chen, W.N., Lu, K.V.** Impact Compressive Response of Dry Sand *Mechanics of Materials* 41 (6) 2009: pp. 777 – 785. https://doi.org/10.1016/j.mechmat.2009.01.003
25. **Zhao, Z., Qiu, Y., Wang, M.** Effects of Strain Rate and Initial Density on the Dynamic Mechanical Behaviour of Dry Calcareous Sand *Shock and Vibration* 2019 2019: pp. 1 – 10. https://doi:10.1155/2019/3526727
26. **Wang, S., Shen, L., Federico, M., Abbas, E.Z., Nguyen, C.N.** Uniaxial Compressive Behavior of Partially Saturated Granular Media Under High Strain Rates *International Journal of Impact Engineering* 102 2017: pp. 156 – 168. https://doi.org/10.1016/j.ijimpeng.2016.12
27. **Felice, C., Gaffney, E., Brown, J., Olsen, J.** Dynamic High Stress Experiments on Soil *Geotechnical Testing Journal* 10 (4) 1987: pp. 192 – 202. https://doi.org/10.1520/GTJ10545J
28. **Yu, X., Ren, W., Zhou, B., Chen, L., Xu, X., Ren, G.** Experimental Study on the Mechanical Behavior and Energy Absorption Capacity of Coral Sand at High Strain Rates *Ocean Engineering* 291 2024: pp. 116343. https://doi.org/10.1016/j.oceaneng.2023.116343
29. **Frew, D.J, Forrestal, M.J, Chen, W.** Pulse Shaping Techniques for Testing Elastic-plastic Materials with a Split Hopkinson Pressure Bar *Experimental Mechanics* 45 (2) 2005: pp. 186 – 195. https://doi.org/10.1007/BF02428192
30. **Bragov, A.M., Lomunov, A.K., Lamzin, D.- A., Konstantinov, A**. Dispersion Correction in Split-Hopkinson Pressure Bar: Theoretical and Experimental analysis *Continuum Mechanics and Thermodynamics* 34 2019: pp. 895 – 907. https://doi.org/10.1007/s00161-019-00776-0
31. **Davies, E.D., Hunter, S.C.** The Dynamic Compression Testing of Solids by the Method of the Split Hopkinson Pressure Bar *Journal of the Mechanics and Physics of Solids* 11 (3) 1963: pp. 155 – 179. https://doi.org/10.1016/0022-5096(63)90050-4
32. **Barr, A.D., Clarke, S.D., Rigby, S.E., Andrew Tyas, A., Warren, J.A.** Design of a Split Hopkinson Pressure Bar with Partial Lateral Confinement *Measurement Science and Technology* 27 (12) 2016: pp. 125903. https://doi.org/10.1088/0957-0233/27/12/125903
33. **Song, B., Chen, W.** Dynamic Stress Equilibration in Split Hopkinson Pressure Bar Tests on Soft Materials *Experimental Mechanics* 44 (3) 2004: pp. 300 – 312. https://doi.org/10.1007/BF02427897
34. **Zhu, J., Hu, S.S., Wang, L.L.** An Analysis of stress Uniformity for Concrete-like Specimens During SHPB Tests *International Journal of Impact Engineering* 36 (1) 2009: pp. 61 – 72.

https://doi.org/10.1016/j.ijimpeng.2008.04.007

35. **Fu, T.T., Zhu, Z.W., Zhang, D., Liu, Z.J., Xie, Q.J.** Research on Damage Viscoelastic Dynamic Constitutive Model of Frozen Soil *Cold Regions Science and Technology* 160 2019: pp. 209 – 221. https://doi.org/10.1016/j.coldregions.2019.01.017
36. **Lv, Y.R., Li, X, Wang, Y.** Particle Breakage of Calcareous Sand at High Strain Rates *Powder Technology* 336 2020: pp. 776 – 786. https://doi.org/10.1016/j.powtec.2020.02.062
37. **Wei, J.Q., Lv, Y.R., Liu, G.Q., Zhang, L., Li, L.** One-dimensional Impact Responses and Energy Absorption of Calcareous Sand *Rock and Soil Mechanics* 40 (1) 2019: pp. 191 – 198+206. (in Chinese). https://doi.org/10.16285/j.rsm.2017.1235
38. **Martin, B.E., Chen, W., Song, B., Akers, S.A.** Moisture Effects on High Strain-rate Behavior of Sand *Mechanics of Materials* 41 (6) 2009: pp. 786 – 798. https://doi.org/10.1016/j.mechmat.2009.01.014
39. **Xiao, Y., Yuan, Z., Chu, J., Liu, H., Huang, H., Luo, S.N., Wang, S., Lin, J.** Particle Breakage and Energy Dissipation of Carbonate Sands Under Quasi-Static and Dynamic Compression *Acta Geotechnica* 14 (6) 2019: pp. 1741 – 1755. https://doi.org/10.1007/s11440-019-00790-1
40. **Veyera, G.E., Charlie, W.A., Hubert, M.E.** One-dimensional Shock-induced Pore Pressure Response in Saturated Carbonate Sand *Geotechnical Testing Journal* 25 (3) 2002: pp. 277 – 288. https://doi.org/10.1520/GTJ11098J
41. **Su, H.Y., X, J.Y., Bai, E.L., Gao, Z.G., Chen, Y.** Experimental Study on Impact Mechanical Response and Statistical Damage Constitutive Model of Ceramic Fiber Reinforced Concrete *Engineering Mechanics* 30 (6) | 2013: pp. 148 – 153. (in Chinese) https://doi.org/1000-4750(2013)06-0148-06
42. **Ouyang, H., Dai, G., Qin, W., Gong, W.** Dynamic Behaviors of Calcareous Sand Under Repeated One-dimensional Impacts *Soil Dynamics and Earthquake Engineering* 12 2021: pp. 106891. https://doi.org/10.1016/j.soildyn.2021.106891
43. **Xiong, Z.M., Lv, S.H., Li, Y.L., Zhao, Q.F., Li, J., Tan, S.S., Jiang, L., Yang, Q.F., Zhang, N.B., Zhang, Z.D.** Research on Dynamic Properties and Energy Dissipation of Loess Under Passive Confining Pressure Conditions *Rock and Soil Mechanics* 42 (03) 2021: pp. 775 – 782+789. (in Chinese) https://doi.org/10.16285/j.rsm.2020.1093
44. **Tong, C.X., Xing, D.P., Hao, Z.B., Feng, J.Y.** Study on Dynamic Mechanical Behavior of Loess under Impact Loading *China Journal of Highway and Transport* 2024: pp. 1 – 16. (in Chinese) http://kns.cnki.net/kcms/detail/61.1313.U.20240116.1105.008.html

Nomenclature

ε_{i} Incident strain, %
ε_{r} Reflected strain, %
ε_{t} Transmission strain, %
$\dot{\varepsilon}$ Strain rate, s^{-1}
σ Stress, MPa
E_0 Elastic modulus of the bars, MPa
A Cross-sectional areas of the bars, m^2
A_{s} Cross-sectional of specimens, m^2
C_0 Wave velocity in the pressure bar, $m{\cdot}s^{-1}$
l_{s} Specimen length, m
E_{50} Equivalent stiffness, MPa
σ_{50} Half the peak stress, MPa
ε_{50} Strain corresponding to σ_{50}, %
w Water content, %
D_{r} Relative density
η Energy density, $MJ{\cdot}m^{-3}$
C Wave velocity in the specimen ($m{\cdot}s^{-1}$)